Eur. Phys. J. Special Topics **227**, 3–16 (2018)

https://doi.org/10.1140/epjst/e2018-00116-7

THE EUROPEAN PHYSICAL JOURNAL SPECIAL TOPICS

Regular Article

Dynamic compaction of polyurethane foam: experiments and modelling

P. Pradel[1,a], F. Malaise[1], T. de Rességuier[2], C. Delhomme[3], G. Le Blanc[4], and J.H. Quessada[1]

[1] CEA CESTA, 15 avenue des Sablières CS60001, 33116 Le Barp Cedex, France
[2] Institut Pprime UPR 3346 CNRS-Université de Poitiers-ENSMA, 11 boulevard Marie et Pierre Curie, 86962 Futuroscope Chasseneuil Cedex, France
[3] CEA LR, BP 16, 37260 Monts, France
[4] CEA GRAMAT, BP 80200, 46500 Gramat, France

Received 6 November 2017 / Received in final form 16 February 2018
Published online 10 September 2018

Abstract. The framework of this paper is to investigate the mitigation ability of an expanded rigid polyurethane foam against extremely fast ($>10^6$ s^{-1}) and intense (>10 GPa) dynamic loadings. Cyclic quasi-static tests and dynamic experiments (gas gun and low inductance generator) have been performed to investigate the foam behaviour for strain rates ranging from 10^{-3} to 10^5 s^{-1}. Analysis of the experimental results shows that the foam has an elastic behaviour phase followed by a compaction phase with significant permanent sets. Compaction threshold is about 8 MPa under quasi-static loading, and 21 MPa for strain rates above 10^4 s^{-1}. A porous compaction model is used to represent the macroscopic behaviour of the foam for the whole range of strain rates. The parameters are identified from dynamic experimental results. The model is validated by comparing calculated velocity profiles with an explicit hydrocode and velocity profiles measured during the experiments.

1 Introduction

Polymeric foams are widely used in automotive [1], marine [2], electronics [3], military [4] and aerospace industries for their thermal insulation or shock mitigation properties. Their energy absorption abilities are particularly useful to develop lightweight shields against impact events or other shock wave loadings. In the case of laser driven experiments, such as the ones performed at the Laser MégaJoule in France or at the National Ignition Facility in the USA, high and short duration stress waves are generated in the experimental chamber by shrapnel impacts or direct laser irradiation. The properties of rigid polyurethane foams would be of great interest to develop protective assemblies to protect some diagnostics or samples support devices.

In this paper, we propose to characterize and to model the dynamic compaction behaviour of a rigid polyurethane foam (320 kg/m^3) by performing shock wave experiments. Numerous experimental studies have already been conducted at low strain

[a] e-mail: pierre.pradel@cea.fr

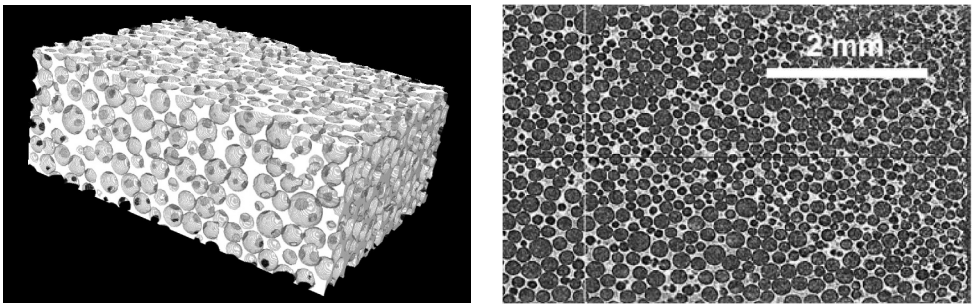

(a) (b)

Fig. 1. Structure of the polyurethane foam obtained by X-ray tomography: (a) three-dimensional reconstruction; (b) cross section.

rates ($<10^3$ s^{-1}). Quasi-static tests [2,5,6] or Split Hopkinson Pressure Bar (SHPB) experiments [2,7] have been performed to study the behaviour of these materials at low strain rates. Few experimental data are available on high density (300 kg/m^3) rigid polyurethane foams at high strain rates [8,9]. Although these experiments are accurate to study the behaviour of the foams at high strain rates, the load durations are not completely representative of laser irradiation or high velocity impacts. That is why the studied polyurethane foam has been tested with gas gun launcher ($\dot{\varepsilon} = 2 \times 10^5$ s^{-1}) and magnetic pressure generator [10] ($\dot{\varepsilon} = 5 \times 10^4$ s^{-1}). Nevertheless, preliminary quasi-static tests have been performed to analyze the foam behaviour for very low strain rates in order to compare with high strain rates.

For this class of material, the response at macroscale depends on the dynamic behaviour of the cell material, the geometry and the size of the cells [11]. In the literature, there are some attempts to predict the behaviour at macroscale from mesoscale or microscale description. The mesoscale modelling is difficult because the properties of the structural material are not well known. It is impossible to machine representative samples at this scale and the properties would greatly depend on the fabrication process. The elastic properties could be predicted by these approaches [11,12], but the non-linear domain due to compaction is not yet well described. On the other hand, the assumption of a homogeneous behaviour in the framework of continuous mechanics can be questioned considering the sharp stress gradients involved in our applications and experiments. Nevertheless, the behaviour of closed-cells polymer foam is well represented by homogeneous mechanical models [13]. The model developed by SRI [14] is particularly suitable to polymer foams, because the compaction domain is defined on experimental data.

2 Material

Polyurethane is the product of the reaction between diisocyanate and alcohol. The foam is obtained by adding water to the mixture. Water reacts with isocyanate to form carbon dioxide gas. The structure of CO_2 bubbles remain after drying process. That explains the spherical geometry of the closed-cells at the end of fabrication (Fig. 1).

The analysis of X-ray tomographies allows to determine the porosity (66%) and the pore size statistical distribution (Fig. 2). The pore diameter is below 200 micrometers, but mainly around 100 micrometers.

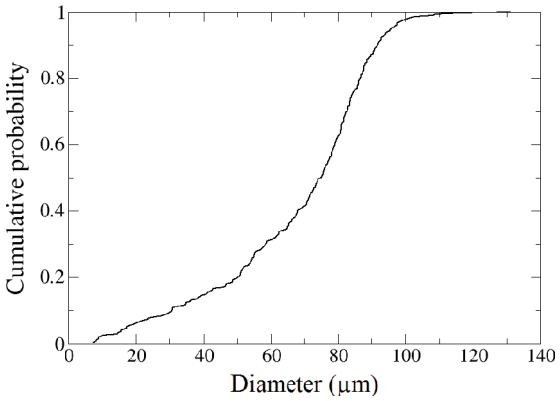

Fig. 2. Pore size distribution in the polyurethane foam.

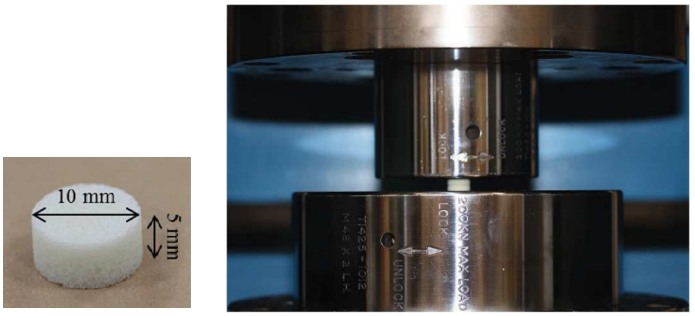

(a) (b)

Fig. 3. (a) Sample of polyurethane foam; (b) sample between the metallic elements of the testing machine.

Cylindrical samples with initial density of 320 ± 20 kg/m^3 were prepared for this study. The diameter is between 10 and 30 mm, and the thickness is from 2 to 5 mm. According to literature data, the density of fully dense polyurethane is 1240 ± 40 kg/m^3. The porosity deduced from the densities is then 74%. Actually, the density of fully dense material is not well-known. The addition of water during the polymerization process may contribute to decrease the density of the structure.

3 Quasi-static tests

Several types of quasi-static compression tests were performed on the Zwick Z330 Red testing machine. The samples are cylinders with 10 mm diameter and 5 mm thickness. All the tests are done at room temperature. The samples were compressed between two metallic elements. The experimental set-up is represented in Figure 3. A pre-load of 3 N is applied at the beginning of the tests to ensure good initial contact at the sample-metal interfaces.

Unconfined and radially confined uniaxial compression tests have been performed. The campaign also includes loading/unloading tests at stress levels from 15 to 500 MPa. Figure 4 shows the uniaxial compression curve obtained under an unconfined test (stress is assumed positive in compression). Tests are reproducible.

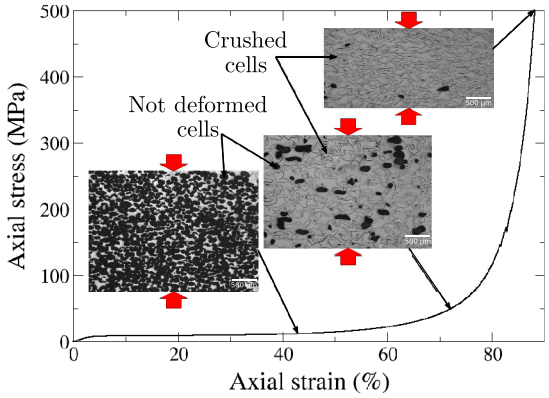

Fig. 4. Engineering stress versus engineering strain and micrographs of cross sections in recovered samples.

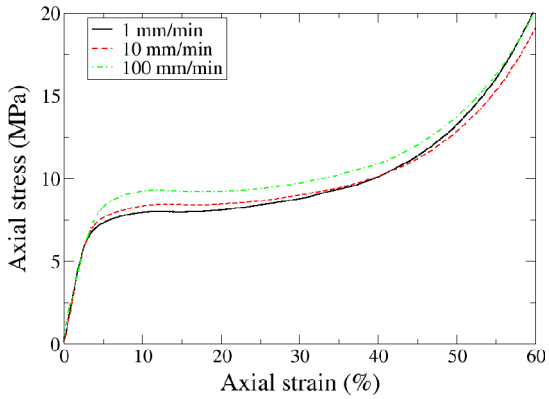

Fig. 5. Engineering stress versus engineering strain for three displacement velocities.

The beginning of the curve is representative of the initial elasticity of the foam. At mesoscale, cells uniformly distort and can retrieve their initial shape. Then, there is a long plateau, with almost constant stress and large strain. It can be attributed to plastic distortion or fracture of the cells. Hence, this deformation is expected to be irreversible on the plateau. At the end of the plateau, most of the cells are collapsed and broken cells are crushed. The final stage is compression of the fully dense material to very high stresses.

Some recovered samples were embedded in a resin, sectioned, polished and observed (Fig. 4). Micrographs confirm the damage of cells under compressive stresses. The dark areas in the micrographs are unbroken cells where the light is lost due to reflection from curved walls. On the other hand, broken (open) cells have been filled up with resin, so they appear as clear zones delimited by slightly darker contours. Their number increases with compression level.

In the former test, the displacement velocity was 1 mm/min, so the strain rate is around 3×10^{-3} s^{-1}. Tests at 10 and 100 mm/min (3×10^{-2} and 3×10^{-1} s^{-1}) have been performed to study low strain rate effects. The results of Figure 5 show that the strain rates do not affect elastic modulus. But the compaction strength (onset of the plateau) is slightly increased.

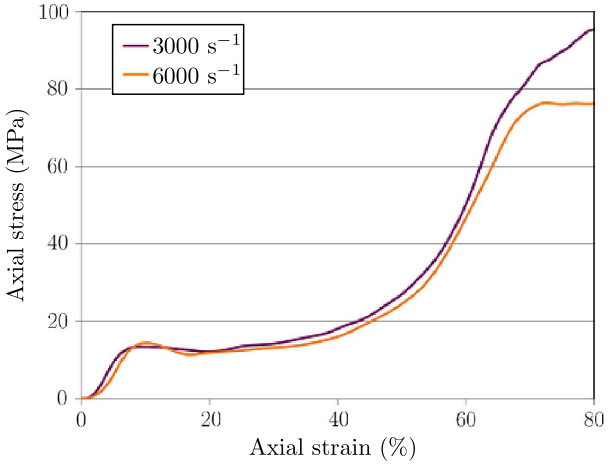

Fig. 6. Engineering stress versus engineering strain for SHPB experiments.

This is corroborated by the results of recent SHPB experiments performed at CEA, at higher loading rates (Fig. 6). The compaction plateau begins at 13 MPa instead of 8 MPa under very low strain rates.

Previously, we indicated that the deformation on the plateau was expected to be irreversible. It is not exactly true as can be seen on the results of cyclic tests presented in Figure 7. These tests have been performed under uniaxial compression loadings without radial confinement to prevent friction at sample/confinement interface. Residual deformation increases under successive compression cycles. It is stabilized after several cycles. The strain at the end of unloading path is different of the strain at the beginning of reloading. We assume that the differences are due to time dependent relaxation of polymer chains or broken fractions of cells, which is responsible of the viscoelasticity of the foam. Such viscoelasticity will not be accounted for in the model since it barely affects the strain values at the end of each unloading.

As the dynamic experiments presented in the next Section are performed under planar shock wave loading, we can consider that we are in conditions of uniaxial strain. Thus, additional quasi-static experiments have been performed using a radial confinement by a steel cylinder in order to compare the quasi-static and dynamic behaviours of the foam under uniaxial strain loading. Figure 8 provides the comparison between the polyurethane response under uniaxial stress and uniaxial strain compression.

The bulk modulus represents the initial slope of the curve and its value is 280 MPa. The compaction plateau is exactly the same until large strain. So, the strain rate effects and the viscoelastic relaxation phenomena shown on unconfined tests would be observed on equivalent confined tests.

4 Dynamic response

Plate impact and magnetic pressure experiments have been performed to identify the behaviour of polyurethane foam under high strain rates (10^4–10^5 s^{-1}).

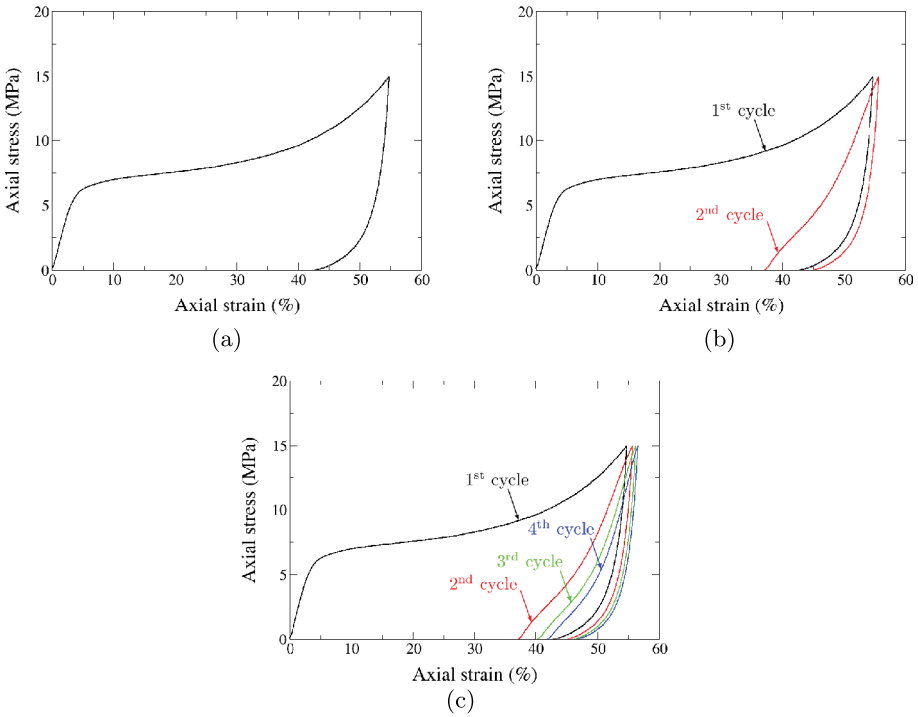

Fig. 7. Stress–strain curves obtained after quasi-static cyclic compression tests up to 15 MPa.

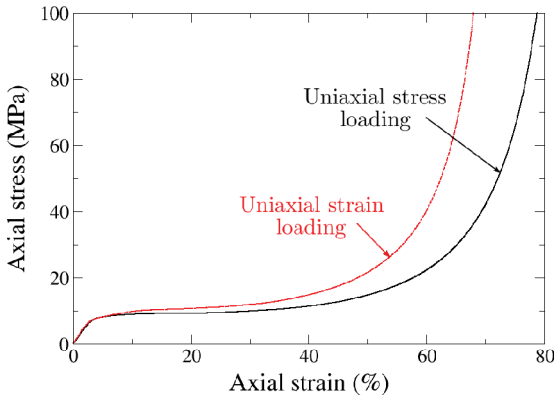

Fig. 8. Engineering stress versus engineering strain for unconfined and confined experiments.

4.1 Magnetic pressure experiments

The electric generator GEPI is a low inductance generator developed by ITHPP and CEA Gramat [10]. A current I outcomes from the release of several capacitors and flows in a strip line (Fig. 9), whose upper and bottom parts are connected by a short

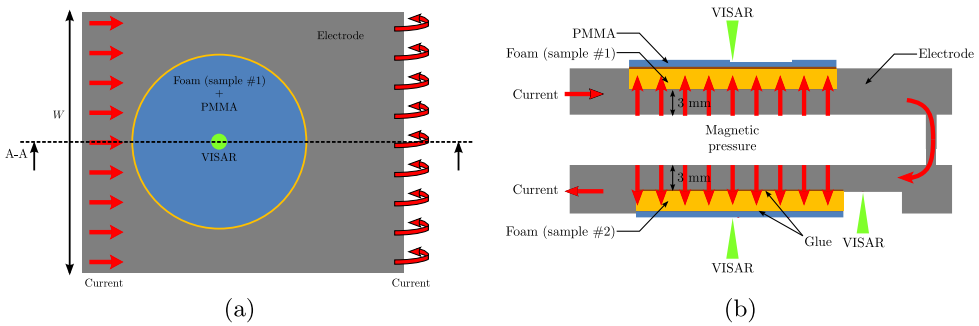

Fig. 9. (a) Top view and (b) A-A side view of GEPI experiments.

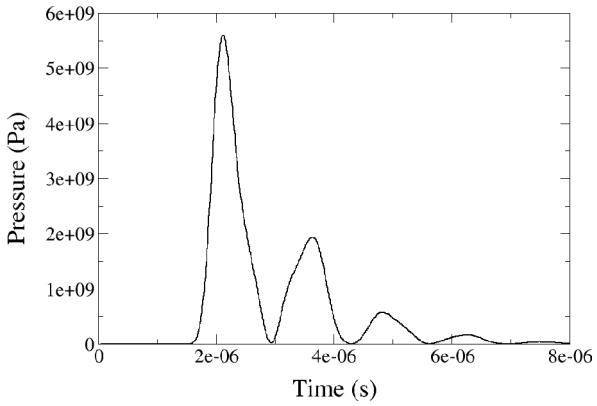

Fig. 10. Pressure profile for GEPI experiments.

Table 1. Characteristics of the GEPI experiment #1271.

Test	W (mm)	$I_{\max}$ (MA)	k_p	$P_{\max}$ (GPa)
1271	30	2.9	0.97	5.7
1272	50	3.0	1.00	2.3

circuit. This current generates, by Laplace effect, a magnetic pressure defined by:

$$P = k_p \frac{B_{th}^2}{2\mu_0} = k_p \frac{\mu_0}{2} \left(\frac{I}{W} \right)^2, \tag{1}$$

where k_p is a scale factor, B_{th} is the magnetic field in a theoretical strip line, μ_0 is the magnetic permeability, I is the current intensity and W is the width of the strip line. The current signal is sinusoidal and can achieve 3 or 4 MA in 600 ns. The shape of the resulting pressure pulse applied to the strip line has a damped sinusoidal shape too (Fig. 10). Strain rates are about 5×10^4 s^{-1}.

The strip line is represented in Figure 9. The upper and the bottom part of the strip line are made of aluminum (Al2024). The width of the strip line is fixed to modulate the level of magnetic pressure: narrow strip line corresponds to maximum pressure (Tab. 1).

The 20 mm-diameter and 2 mm-thick foam samples are glued between the 3 mm-thick strip line and a 1 mm-thick PMMA buffer with epoxy resin. The thickness

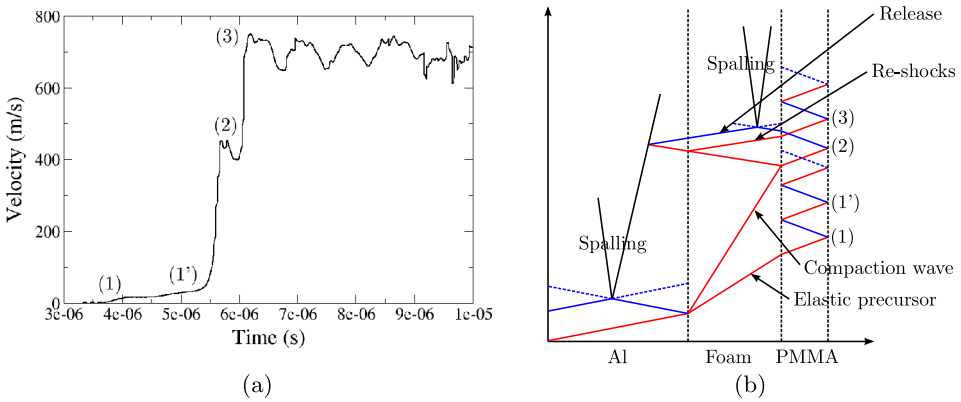

Fig. 11. (a) Velocity history at the PMMA buffer free surface; (b) time-distance diagram for the GEPI experiment #1271.

of the glue is almost 40 micrometers. The velocity histories at strip line and buffer free surface (coated with a thin reflecting layer) were measured by using Velocity Interferometer System for Any Reflector (VISAR). The velocity at strip line free surface permits to calibrate the coefficient k_p very accurately.

The velocity profiles measured at rear surface of the buffer (Fig. 11) are used to investigate the dynamic compaction of polyurethane foam. The time-distance diagram permits to understand the propagation and interactions of the various waves. Elastic (not represented for simplicity) and plastic waves propagate through the aluminum strip line. The shock transmitted to the foam splits into elastic and compaction waves. The velocities of these two waves are different. They are related to the slope of the pressure-density curve. The confined compression of Figure 8 is not consistent with the dynamic experimental data. The celerity of elastic wave deduced from quasi-static data is weaker than the one from shock experiments (1250 m/s). The corresponding dynamic bulk modulus is 500 MPa.

A release wave is reflected in aluminum. The interaction of this reflected wave with the unloading of magnetic pressure induces spalling inside the strip line. Further wave propagation in the three-layered assembly produces successive accelerations of the PMMA free surface (bold numbers in Fig. 11), which will be used to test the model presented in the next section.

4.2 Plate impact experiments

Plate impact experiments have been performed on a gas gun launcher based at CEA CESTA to apply higher loading rates on foam samples. The experimental configuration is represented in Figure 12 and in Table 2. The projectile is made of polyethylene sabot and PMMA impactor (90 mm diameter). A PMMA drive plate is put in front of the foam samples. It permits the determination of impact velocity and tilt at impact by free surface velocity measurements (not represented). The 30 mm-diameter and 2 mm-thick foam samples are inserted between the drive plate and PMMA windows. The diameter of the bore is large enough to test three foam samples on the same shot. The response of the foam is inferred from the velocity profiles measured at foam/window interface. All these measurements were performed using VISAR and Heterodyne Velocimetry (Het-V, often referred to as PDV). Strain rates are about 2×10^5 s^{-1}.

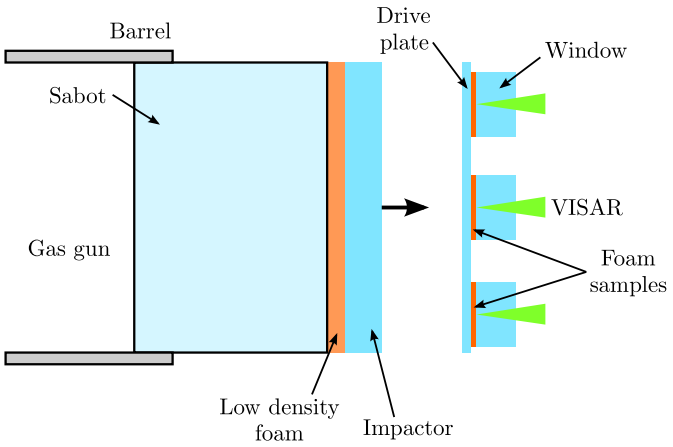

Fig. 12. Scheme of plate impact experiments.

Table 2. Characteristics of the plate impact experiment #9–16.

Test	Impactor		Impact velocity (m/s)	Target	
	Material	Thickness (mm)		Materials	Thickness (mm)
9–16	PMMA	12	282	PMMA/Foam/PMMA	1/2/15
10–16	PMMA	12	388	PMMA/Foam/PMMA	1/2/15
5–17	PMMA	12	405	PMMA/Foam/PMMA	4/2/15

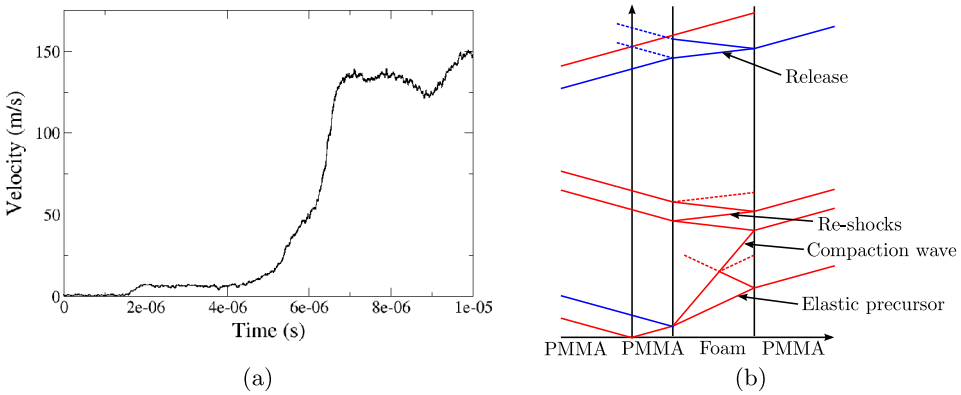

Fig. 13. (a) Velocity history at the foam/window interface; (b) time-distance diagram showing planar wave propagation in the plate impact experiment #9–16.

The velocity profiles measured at foam/window interface are presented in Figure 13. They confirm the increase of the elastic precursor celerity under high strain rates. The velocity of the plateau is also consistent with GEPI experiments one.

An elastic precursor wave first arrives at the interface. It is followed by a compaction wave as seen on the time-distance diagram. Because of re-shock generation at foam/window interface (since the shock impedance of PMMA is higher than that of the foam), it is not accurate to determine the dynamic compaction strength by impedance matching methods, because the behaviour of the compacted foam is

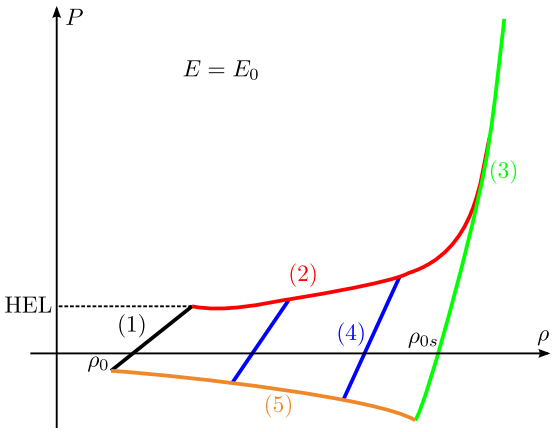

Fig. 14. Scheme of the SRI model for a constant energy $E = E_0$.

not known. Instead, we have used a method based on matching experimental and numerical velocity profiles (see Sect. 6).

5 Phenomenological model

The dynamic behaviour of the foam is represented by a phenomenological model [14] initially developed by the Stanford Research Institute (SRI). This model is based on the Mie Gruneisen equation of state (EOS) of the fully dense material. The response of the foam from its initial state to fully dense material is defined by the initial elasticity, the (plastic) compaction and eventually damage (Fig. 14).

The elastic response (1) is described by Hooke's law using the initial bulk modulus K_0 and the initial density ρ_0 of the foam. The equilibrium compaction curve (2) is defined by a piecewise-polynomial function. It intersects the initial elastic path at the Hugoniot Elastic Limit (HEL). After consolidation, the behaviour of the foam is the same as the fully dense foam one (3). Upon unloading from a partially densified state, the release path is on intermediate surface (4) defined by Mckenzie elasticity of porous materials [15]. Finally, if the release takes the material into sufficient tension (negative pressure), damage can occur and the re-opening of the cells is driven by the damage curve (5). As the tensile strength of the foam is lower that the fully dense material one, the model considers that the slope of the damage curve is negative. Thermal softening is also taken into account by multiplying each equation which describes the different parts of the pressure-density curve by the function $f(E)$. It is calibrated by Dynamic Mechanical Analysis (DMA). The value of $f(E)$ is 1 when the energy is equal to the initial energy and 0 at vitreous transition temperature. The SRI model has been implemented in an explicit 1D hydrocode of CEA. The 1D approach is enough since the experiments have been performed in conditions of uniaxial strain. The parameters of the SRI model are given in reference [16].

First, the parameters of the model have been adjusted to fit the confined quasi-static compression curve. Hugoniot data for polyurethane foam and fully dense material can be found in a Los Alamos Report [17]. These data have been obtained by explosively driven experiments, involving very high stresses. The comparison between experimental data and this "quasi-static version" of the model is shown in Figure 15.

However, as shown in Figure 16, the compaction threshold, determined thanks to measurement of the velocity of the elastic precursor on velocity profiles, increases

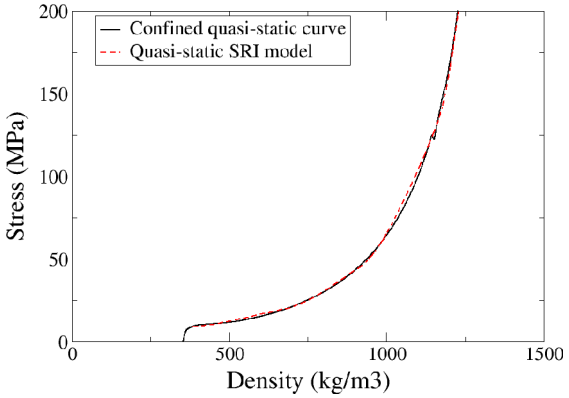

Fig. 15. Compaction curve of the SRI model fitted on quasi-static stress–strain curve.

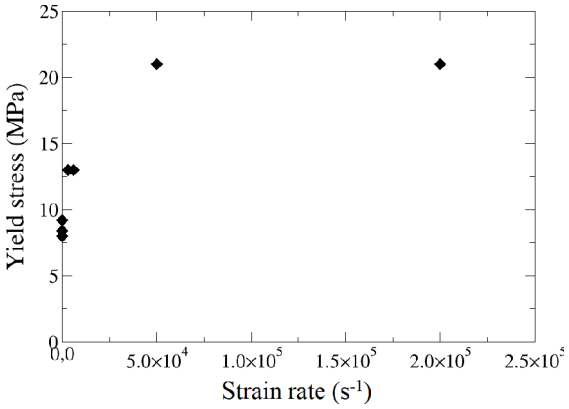

Fig. 16. Yield stress versus strain rate.

between the strain rates of 3×10^{-3} s^{-1} (quasi-static tests) and 5×10^{4} s^{-1} (GEPI experiments), but remains approximately constant equal to 21 MPa above 5×10^{4} s^{-1}. Thus, as the compaction model does not take into account the strain rate, some parameters have been modified to take into account dynamic experimental data, after an optimization procedure. As we are interested only in the restitution of dynamic experiments, we implement a unique model based on GEPI and plate impact experiments. The new elastic and compaction paths are represented in Figure 17.

6 Discussion

The compaction model is implemented into a dynamic explicit unidimensional hydrocode. Both plate impact and magnetic pressure experiments are simulated. Comparisons of experimental and numerical results are presented in Figures 18 and 19. Quasi-static and SHPB experiments are not simulated because the output data (stress–strain curves) correspond to the ones that we enter in the model.

The time arrival of elastic and compaction curves are not well reproduced by the computations with the compaction model fitted on quasi-static data (Figs. 18a and 19a). The correlations between numerical and experimental results are better by using the corrected, “dynamic” compaction model (Figs. 18b and 19b).

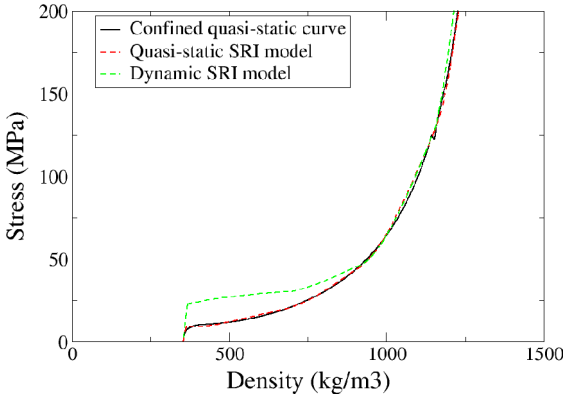

Fig. 17. Comparison of dynamic and quasi-static compaction curves.

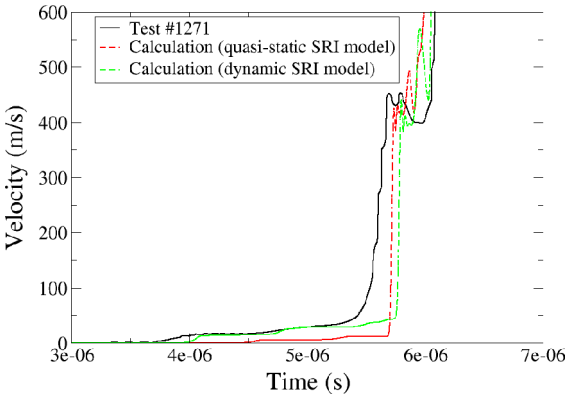

Fig. 18. Comparison of measured and calculated velocity at the buffer free surface for the GEPI experiment #1271 with quasi-static (a) and dynamic (b) SRI models.

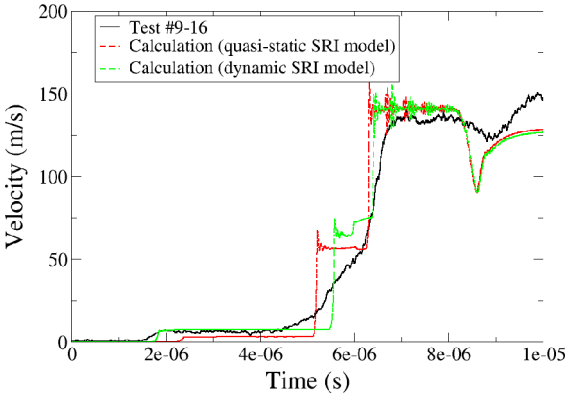

Fig. 19. Comparison of measured and calculated velocity at the foam/window interface for the plate impact experiment #9–16 with quasi-static (a) and dynamic (b) SRI models.

For the GEPI experiment #1271, the first two plateaus (<50 m/s) are well reproduced which means that the elastic precursor is correctly calculated. The next acceleration corresponding to the compaction wave is well reproduced, which is not the case of the final velocity, after reflections in the buffer and at the aluminum/foam interface. Actually this final velocity was observed to depend on the value of the spall strength of aluminum. The calculated times arrival are however consistent, which means that the compaction curve is correct.

For the plate impact experiment #9–16, the PMMA impactor initially impacts the drive plate at 282 m/s. The dynamic model correctly represents the elastic precursor and the amplitudes of the other accelerations. The times arrival are well calculated, which validates the shape of the compaction curve. However, the compaction wave front is much steeper in the calculation than in the measured profile. This might suggest a viscoplastic response of the foam not accounted for in the current model.

The bulk modulus and the compaction strength depend on strain rates. Logically, the recommended values are the dynamic ones to simulate shock waves propagation and attenuation. Both plate impact and GEPI numerical simulations are in correct accordance with experimental results. Thus, the compaction strength seems constant from 10^4 to 10^5 s^{-1}. These results have recently been confirmed by laser driven experiments performed at Institut Pprime (France).

7 Conclusion

The framework of this paper was to investigate the mitigation ability of an expanded polyurethane foam against intense and brief stress waves. Quasi-static tests were used to identify compaction mechanisms. Like most porous materials, the foam has an elastic behaviour followed by a compaction phase. Compaction threshold is about 8 MPa under quasi-static loading. Pore closure is due to buckling and fracture of the matrix, which should induce permanent densification. Still, these tests also showed that a part of this deformation is recovered, which indicates a viscoelastic behaviour of the foam. Strain rate effects on compaction mechanisms were investigated by using a gas gun and a low inductance generator. It was found that the compaction threshold increases between the strain rates of 10^{-3} and 10^4 s^{-1}, but remains approximately constant equal to 21 MPa above 10^4 s^{-1}. A porous compaction model was used to represent the macroscopic mechanical behaviour of the foam. The parameters were identified from velocity profiles measured during dynamic experiments. Times arrival of the waves and velocity levels are fairly consistent, which shows the ability of such model to represent compaction mechanisms at high strain rates.

Further work will consist in performing dynamic experiments on the polyurethane foam for strain rates above 2×10^5 s^{-1} (electron beam and laser-driven shock experiments). They will be used to confirm the evolution of the compaction threshold and the validity of the compaction model for such strain rates.

References

1. F.A.O. Fernandes, R.T. Jardin, A.B. Pereira, R.J. Alves de Sousa, Mater. Des. **82**, 335 (2015)
2. A. Pellegrino, V.L. Tagarielli, R. Gerlach, N. Petrinic, Int. J. Impact Eng. **75**, 214 (2015)
3. S.H. Goods, C.L. Neschwanger, C. Henderson, D.M. Skala, Mechanical properties and energy absorption characteristics of a polyurethane foam, Technical report, Sandia National Laboratories, 1997

4. J.C. Gowda, A flexible syntactic foam for shock mitigation, Ph.D. thesis, North Carolina A&T State University, 2011
5. H. Jmal, Identification du comportement quasi-statique et dynamique de la mousse de polyuréthane au travers de modèles à mémoire, Ph.D. thesis, Université de Haute Alsace, 2012
6. Z.H. Tu, V.P.W. Shim, C.T. Lim, Int. J. Solids Struct. **38**, 9267 (2001)
7. W. Chen, F. Lu, N. Winfree, Exp. Mech. **42**, 65 (2002)
8. E. Zaretsky, Z. Asaf, E. Ran, F. Aizik, Int. J. Impact Eng. **39**, 1 (2012)
9. D.M. Dattelbaum, J.D. Coe, C.B. Kiyanda, R.L. Gustavsen, B.M. Patterson, J. Appl. Phys. **115**, 174908 (2014)
10. P.L. Hereil, F. Lassalle, G. Avrillaud, AIP Conf. Proc. **706**, 1209 (2004)
11. L.J. Gibson, M.F. Ashby, *Cellular solids: structure and properties – second edition* (Cambridge University Press, 1997)
12. F. Saint-Michel, L. Chazeau, J.Y. Cavaillé, E. Chabert, Compos. Sci. Technol. **66**, 2700 (2006)
13. P. Pradel, F. Malaise, T. de Rességuier, C. Delhomme, B. Cadilhon, J.H. Quessada, G. Le Blanc, Stress wave propagation and mitigation in two polymeric foams, in *Proceedings of the 2017 APS-SCCM conference* (2017)
14. L. Seaman, R.E. Tokheim, D.R. Curran, Computational representation of constitutive relations for porous materials, Technical report, Stanford Research Institute, 1974
15. J.K. Mckenzie, Proc. Phys. Soc. **63**, 2 (1950)
16. P. Pradel, Étude de la compaction dynamique de mousses polymères : Expériences et modélisation, Ph.D. thesis, École Nationale Supérieure de Mécanique et d'Aérotechnique, 2017, https://tel.archives-ouvertes.fr/tel-01737770v1
17. S.P. Marsh, *LASL shock Hugoniot data* (University of California Press, 1980)